Double *K*-shell photoionization of silver

E. P. Kanter, I. Ahmad, R. W. Dunford, D. S. Gemmell, B. Krässig, S. H. Southworth, and L. Young
Argonne National Laboratory, Argonne, Illinois 60439, USA

(Received 3 June 2004; revised manuscript received 20 September 2005; published 7 February 2006)

We have investigated double *K*-shell vacancy production in x-ray photoionization of silver. Measurements were carried out with photon energies (50–90 keV) varying from below threshold to beyond the expected maximum of the double *K*-shell ionization cross section. The limit of asymptotically high energies was deduced from measurements of double *K*-shell ionization following *K*-electron capture by ^{109}Cd nuclei. The photon energy dependence of the ratio of double to single *K* vacancies produced is compared to similar measurements in helium and models thereof. The dependence of that ratio on atomic number is assessed by combining these data with previous experimental and theoretical estimates. The results show a clear growth in the relative importance of the dynamical electron-electron scattering contribution in heavy atoms.

DOI: 10.1103/PhysRevA.73.022708 PACS number(s): 32.80.Fb, 31.25.Eb, 32.30.Rj, 31.10.+z

I. INTRODUCTION

Double *K*-shell photoionization of an atom, in which a single photon is absorbed liberating both *K* electrons, creates a "hollow atom." The simplest example of double *K*-shell photoionization is the case of helium, which has been extensively studied ever since the first reported measurement more than 30 years ago [1]. Because of the single-particle nature of the photon-electron dipole operator [2], double ionization would not occur in the absence of the *e*-*e* interaction and thus this process serves as an extremely sensitive probe of electron correlations within atoms [3,4]. There has been considerable progress both experimentally and theoretically in understanding the problem in helium [5] and workers have now turned to methods of investigating such processes in other systems as a more extensive test of the theories. Experimentally, this has been difficult to achieve in all but the lightest heliumlike systems ($Z \leqslant 3$) [6]. In atomic spectroscopy, it is usually argued that electron-electron correlations are less important in heavier atoms because of the dominance of the electron-nucleus interaction over the electron-electron interaction. While this is certainly true in determining energies, the effect on double *K*-shell ionization is quite different. Because double ionization proceeds through the *Z*-independent *e*-*e* interaction, the effects of electron-electron correlations have been found to be persistent in heavy atoms [7] and consequently more challenging to treat in high-*Z* systems where relativistic effects simultaneously become important [8].

Because of the relative isolation of the *K*-shell electrons from the outer-shell electrons in heavy atoms, the double *K*-shell ionization of a heavy atom, producing a hollow atom, is comparable to the double ionization of the same heliumlike system, stripped of the outer shell electrons. Here, we used a relatively simple method to probe the effects of electron-electron correlations in the *K* shell of a heavy atom by the creation of double *K* vacancy states in x-ray photoionization of silver and subsequent detection through the observation of the coincidence between the hypersatellite and satellite transitions as those states relax.

The formation and decay of atoms with multiple vacancies was first considered by Heisenberg [9] during the early development of quantum mechanics. Double *K*-shell ionization became an important subject in nuclear physics because of the predictions of Migdal [10] and Feinberg [11] of the production of such atomic systems in nuclear α and β decay processes. For $Z > 40$, where *K*-fluorescence yields are large, the dominant decay of double *K* vacancy states is through the sequential emission of two *K* x rays.

In 1953, Charpak [12] first observed such x-ray cascades following the electron capture (EC) decay of ^{55}Fe by coincident detection of the x rays in a pair of proportional counters. Since that time, many workers have investigated the production and decay of hollow atoms in α, β, electron capture, and internal conversion (IC) decays of radioactive nuclei [13]. Briand *et al.* [14] were the first to point out the large energy shifts (from the normal diagram lines) of the $K^{-2} \rightarrow K^{-1}L^{-1}$ transitions. They termed these *hypersatellites* in contrast to the more common *satellite* transitions arising when, in addition to a single *K* vacancy, there are one or more additional vacancies in the *outer* orbitals of the initial state. Using radioactive sources, several atomic structure aspects of such decays have been investigated including the suppression of the $K\alpha_1$ transition [15], relativistic effects [16], and the importance of electron-electron correlations [7]. Observations of hollow atoms have also been made using fast electron impact [17] and ion-atom collisions [18,19]. Such experiments have also produced a wealth of high-quality data on hypersatellites; however, these probes produce additional ionization in outer shells and result in complex spectra and do not help elucidate the production mechanism in photoionization.

The data from measurements with radioactive sources are cleaner than those from charged particle impact and have been illuminating for our problem but also somewhat limited because of the range of sources available. Due to the change in nuclear charge in α, β, and EC decays, shake-up and shake-off processes dominate the production of double *K* vacancies with such sources. In contrast, in IC decays, the Coulomb field of the nucleus remains essentially unchanged and, especially near threshold, there can be substantial contributions from correlated electron motions. Unfortunately, with IC, the exciting photon (in this case virtual) is of *fixed* energy. Previous attempts to study hypersatellite production

in photoionization using x-ray tubes have been hampered [20,21] because of the limited photon flux and tunability. In order to study both the energy and atomic number dependence, photoionization measurements at synchrotron x-ray sources are vital.

In recent years, several groups have exploited modern synchrotron radiation sources to probe the formation and decay of such double K vacancy states with tunable x rays [22–26]. In the present work, we have extended those experiments to Ag (Z=47), the heaviest element yet studied with synchrotron radiation. We chose to study silver because of extensive measurements which have been previously carried out using the EC decay of ^{109}Cd in a radioactive source [27] producing hollowed ^{109}Ag. By combining our measurements with those previous data, we have been able to probe the energy dependence of the double K ionization probability from threshold to asymptotically high energy.

II. THEORETICAL BACKGROUND

For He, extensive use has been made of many-body perturbation theory [28–31] and methods have been developed to treat the problem of two correlated outgoing electrons exactly [32]. No similar calculations exist for heavy atoms. There is another, more scalable, approach which allows a physical interpretation and provides a means to compare our results in Ag to theory. In this approach [33], two primary processes are considered: electron-electron scattering (or KO for knock-out) and shake (or SSO as described in the sudden approximation [34]). These contributions can be separated by exploiting their very different classical or quantum natures. Schneider and Rost have argued that, while electron-electron scattering can be described classically, there is no classical analog of shake processes which must be treated quantum mechanically [35]. They further showed that KO and SSO can be experimentally isolated because of their very different energy dependences. Because of the strong energy dependence of electron-electron scattering, KO is most prominent at lower energies, falling rapidly with increasing energy. In contrast, at higher energies (where KO is negligible), double photoionization of the K shell has been discussed extensively in terms of shake processes where a fast photoelectron leaves with most of the available energy and then as the core-excited atom relaxes the second electron is shaken up or off, leading to the concept of an energy-independent asymptotic limit of the ratio between double and single ionization [36,37]. The studies of double K ionization following EC decay of radioactive nuclei provide a useful resource in this endeavor. Because one of the electrons is absorbed in the nucleus, there is only a single free electron in the double K final state following EC, and thus double K ionization proceeds by a pure shake-off process in the extreme limit of the sudden approximation. Hence, the asymptotic limit is determined independently by these EC radioactive source measurements.

III. EXPERIMENT

Experimentally, the unambiguous signal for detecting the presence of double K vacancy states is a hypersatellite transition when the double vacancy state decays. For low $Z(\lesssim 20)$, when fluorescence yields are low, the best method has been high-resolution Auger electron spectroscopy as was recently demonstrated in the case of Ne (Z=10) [26]. As a practical matter, however, this technique has been limited to low-Z gaseous targets. The $K^{-2}\rightarrow K^{-1}L^{-1}$ hypersatellite shift increases with increasing atomic number Z (see Fig. 1), while the fluorescence yields also grow with Z [40]. Thus, for $Z\gtrsim 20$, high-resolution x-ray spectroscopy becomes preferable and permits work with solid targets. This was recently demonstrated by Diamant and collaborators in a beautiful series of experiments at the NSLS at Brookhaven National Laboratory [23,24]. Using a curved-crystal spectrometer, they measured the Cu $K^h\alpha_{1,2}$ hypersatellite emission spectrum following double K-shell photoionization by 18–25 keV photons. Similar measurementshave since been reported for Ca, Ti, and V (Z=20, 22, 23) with photons in the range of 8–35-keV from SPring-8 [25].

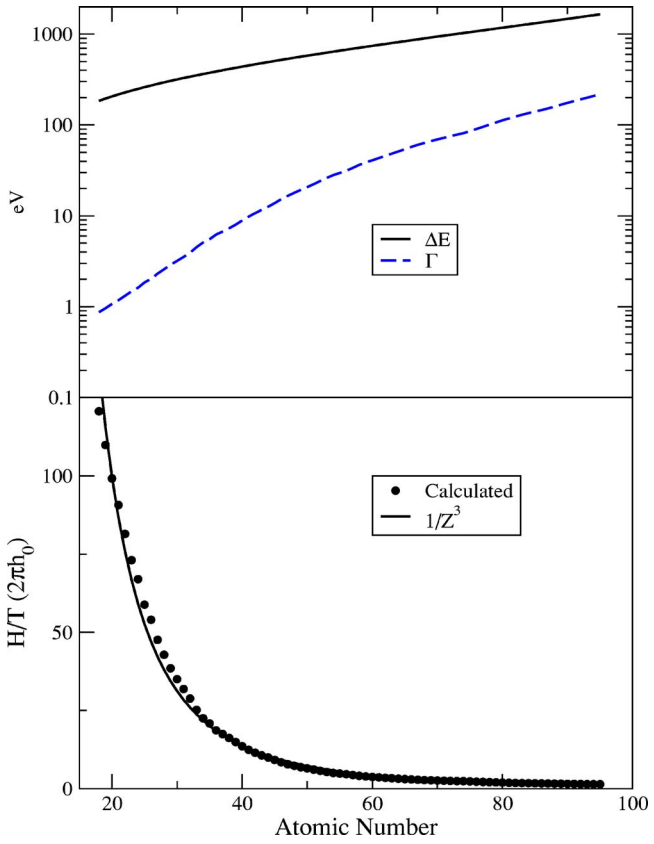

FIG. 1. (Color online) The upper panel shows calculated dependence on atomic number of the hypersatellite-diagram line energy shift (ΔE) [38] and lifetime width (Γ) of the single K vacancy [39]. The lower panel shows the ratio of the hypersatellite yield (H) to the diagram line tail (T) at the position of the $K^h\alpha_1$ peak. The points are the result of the calculation described in text and the line shows a $1/Z^3$ dependence fitted to those points.

That method is very appropriate for such mid-Z elements, but becomes problematic for heavier atoms. This is because asymptotically, the ratio of double to single K photoionization is expected to fall off as h_0/Z^2 (where h_0 is an arbitrary constant), as is observed for shake-off. On the other hand, the natural line width of the diagram line (Γ) grows rapidly

with Z while the hypersatellite energy shift from the diagram line (ΔE) also increases, but more slowly with Z [38] as shown in Fig. 1. If we assume ideal resolution, then the ratio of the total, hypersatellite yield (H) to the Lorentzian tail of the diagram line (T) would be of the form

$$\frac{H}{T} = 2\pi h_0 \frac{\Delta E^2 + (\Gamma/2)^2}{\Gamma Z^2}. \quad (1)$$

Using the atomic level widths given by Keski-Rahkonen and Krause [39], the net result is that with increasing Z, the hypersatellite yield to diagram tail intensity ratio is numerically found to fall off approximately as a $\sim 1/Z^3$ power law (Fig. 1) and thus the tail of the diagram line becomes the limiting background for such singles measurements, regardless of improvements in resolution or angular acceptance. Taking into account the finite resolution of the crystal spectrometer and the natural width of the hypersatellite line, the hypersatellite *peak intensity* to diagram tail ratio will fall even faster with increasing Z. This means that single photon techniques become increasingly difficult in the heaviest atoms. In this regime, coincidence techniques provide a means to isolate the hypersatellite transitions from the far more intense diagram lines. The coincidence technique requires the use of more efficient detectors, so we turn to germanium detectors which provide larger solid angle than the high-resolution crystal spectrometers and adequate resolution for resolving the hypersatellite line from the diagram lines.

In 1999, we observed the double ionization of the K shell of a heavy atom (molybdenum, $Z=42$) photoionized by synchroton radiation [22]. We used the method of satellite-hypersatellite coincidences, pioneered by Briand and collaborators [14]. Following $K^h\alpha\beta$ emission, there is still a single K vacancy and an additional $2p$ or $3p$ vacancy as well. In heavy atoms, the single vacancy decays promptly with the emission of a K x-ray satellite and the coincidence between the hypersatellite and satellite lines provides a discriminating filter against the $\sim 10^5$ times more intense $K\alpha_{1,2}$ diagram lines produced by single K-shell photoionization. The present measurements used the same technique.

The experiment was carried out on the 12-BM bending magnet beamline [41] of the Basic Energy Sciences Synchroton Radiation Center (BESSRC) at the Advanced Photon Source (APS). Photon beams from 50.6 to 90.0 keV were obtained using third-order reflections from a Si(111) double crystal monochromator ($\delta E/E \simeq 2\times 10^{-4}$ for first order) and then transported through vacuum to the experimental hutch. The beam exited the vacuum through a Be window into air and was then collimated with a set of slits to produce a 1×1 mm^2 beamspot at the target. The intense first-order radiation was absorbed by a 5/16-in. aluminum filter leaving primarily third-order radiation with slight contamination ($<10\%$) from fourth, fifth, and seventh orders. These higher orders were further reduced by additional absorbers including Mo, Y, Au, Ta, and Lu of thicknesses chosen to maximize the ratio of the third order to higher-order radiation at each energy. Typically, the third-order flux impinging on the target was $\sim 4\times 10^7$ photons/s. The target consisted of a 20-μg/cm^2 film of natural silver deposited on a 5-μg/cm^2 carbon foil and oriented with the surface normal at an angle of 60° (in the horizontal plane) with respect to the incident beam. The path length in air from the vacuum window to the target was approximately 1 m.

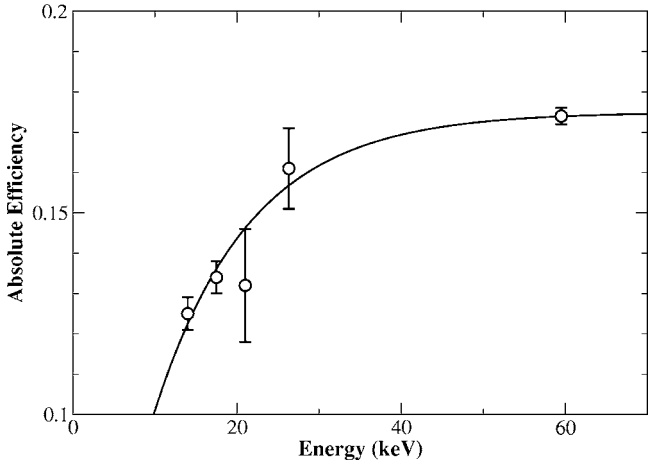

FIG. 2. Measurements of the absolute photopeak efficiency for one of the Ge detectors with a calibrated ^{241}Am source. The line is drawn to guide the eye.

Two 5 cm$^2\times 1$ cm Ge low-energy photon spectrometers (LEPS's) faced each other and were normal to the beam, lying in the same plane as the beam polarization and the target normal. With this geometry, Compton and Rayleigh scattering were suppressed. These suppressions are desirable to reduce the detector count rates and background coincidences from Compton scattering off of the K shell. Each detector was covered with a 127-μm Kapton filter to suppress high-energy photoelectrons produced by the residual higher-order components of the beam while transmitting the $\sim$21–26-keV Ag $K\alpha,\beta$ x rays with $>99\%$ probability. The energy resolutions of the two detectors were 340 and 350 eV (full width at half maximum) at 26 keV. The face of each detector was $\sim$5 mm from the beam, and the active Ge crystals were further displaced $\sim$11 mm from the Kapton face. This gives a solid angle of $\sim$1.4 sr for each detector for a combined 22% angular efficiency. In order to better determine the geometry, additional efficiency measurements were carried out with a calibrated ^{241}Am source placed at the intersection of the beam with the target. These measurements served to determine the energy-dependent absolute efficiencies of the detectors including absorption in the Kapton filters, Be detector windows, and crystal surface electronic contacts as well as the angular efficiency. An example for one of the detectors is shown in Fig. 2. Based on these measurements, the actual combined angular efficiency of the two detectors was found to be 27% of 4π.

Standard coincidence electronics recorded the energies deposited in each detector and the time difference between the detectors for all coincidence events within 5 μs (see Fig. 3). This time window was sufficiently broad to encompass the $\sim$3.7-μs revolution period of the electrons in the storage ring. In addition to all coincidence events, 1% of all singles events were also recorded. Total count rates were generally maintained in the range of 2–4 kHz in each detector by retuning the second monochromator crystal orientation as the

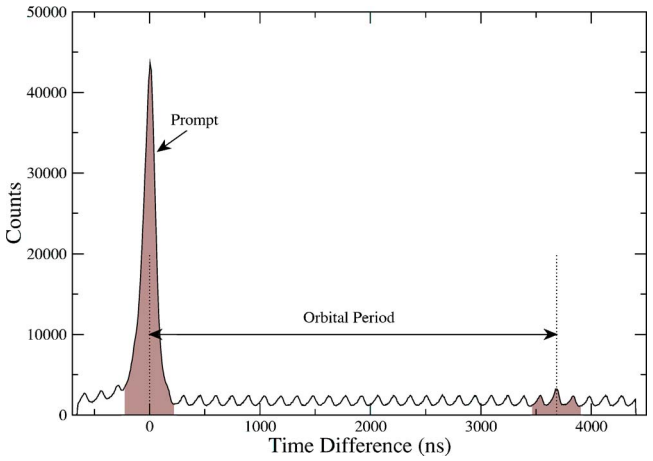

FIG. 3. (Color online) A typical distribution of time difference between the two Ge detector signals for coincidence events. The regions defining the "prompt" (time difference=0) and "delayed" coincidences are shaded.

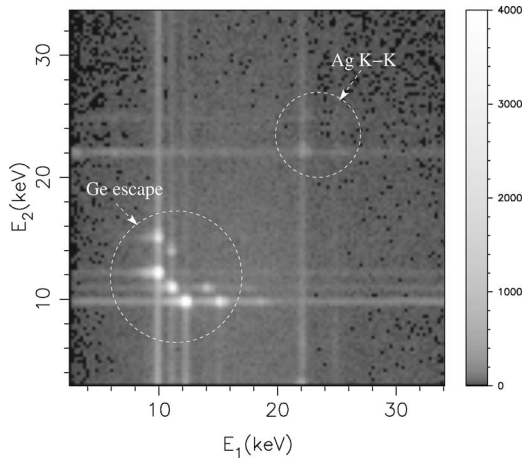

FIG. 4. Prompt coincidence energy spectrum for double *K*-shell photoionization of Ag by 90-keV photons displayed as a gray scale contour plot. The axes represent the energies measured in each detector. Both the double *K* coincidence (22–25 keV) and the Ge escape peak regions are indicated.

storage ring current decayed with each fill. Overall recorded event rates were ~100 Hz, and the computer dead time always <1%. Because of the complex microstructure of the electron bunches in the storage ring (there were 28 bunches with various time spacings ranging from 2.4 to 460 ns, though 153 ns was the most probable, corresponding to 21 of the 28 gaps), the accidental delayed coincidences are modulated and produce a series of peaks and troughs with the predominant 153 ns periodicity in the time difference spectrum (see Fig. 3). "Prompt" coincidences were defined by timing signals from the two detectors within ±220 ns of each other. "Delayed" coincidences were defined by that same 440-ns time window in the time difference spectrum shifted by one orbital period of the storage ring. Those timing windows are indicated by the shaded regions in Fig. 3.

Because the large-area Ge detectors were placed so close together, there was a substantial probability for the escape of Ge fluorescence from one detector and subsequent detection of that fluorescence in the other detector (see Fig. 4).This is a common problem in coincidence experiments with Ge detectors in this energy range and is usually addressed by reducing the solid angle for one detector observing the other (see, e.g., [42]). In this experiment, however, the escape coincidences were only moderately more intense than coincidences with Ag *K* x-ray fluorescence (see Fig. 5) and well separated in energy (~10 keV) from the Ag *K* region including the satellites and hypersatellites, so this was deemed an acceptable geometry that did not sacrifice coincidence efficiency.

An additional source of coincidence background could come from two-atom emission events produced by electron impact ionization. Because the double *K*-shell ionization threshold (E_{2K}=51.782 keV) is more than twice the single *K*-shell ionization threshold (E_{1K}=25.514 keV), the photoelectrons resulting from single ionization of one atom are always sufficiently energetic to ionize the *K* shell of another atom. Such events could produce coincidences between two *K* x-ray diagram lines. Such events are ultimately distinguishable from the hypersatellites because of the ~600 eV shift of the latter. However, to reduce such a background, we sought to minimize secondary collisions by using a thin Ag target (20-μg/cm^2 ≃ 19 nm). This is much thinner than the shortest mean free path for electron impact ionization of the *K* shell by 25–80-keV electrons which is estimated to be ~2550 μm [43]. The absence of this background was tested by comparing a measurement at a photon energy below $2E_{1K}$ and another at a photon energy intermediate between $2E_{1K}$ and E_{2K}. The consistency of those two measurements demonstrated that there was no appreciable contribution from this background source.

The other major sources of coincidences came from x-ray cascades following photoionization and Compton scattering from the *K* shell. The former produces coincidences between *K* and *L* x-ray diagram lines which are easily separated energetically. The latter produces coincidences between a *K*

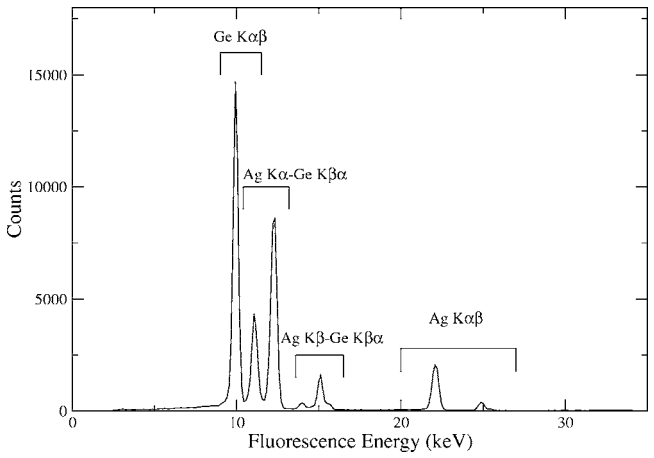

FIG. 5. Fluorescence energy spectrum observed in one of the detectors for coincidence events showing the regions of Ag $K\alpha\beta(\equiv K\alpha+K\beta)$ emission and Ge escape peaks (corresponding to projection on the *x* axis for a spectrum such as shown in Fig 4). These data were taken with 61.5-keV incident photons.

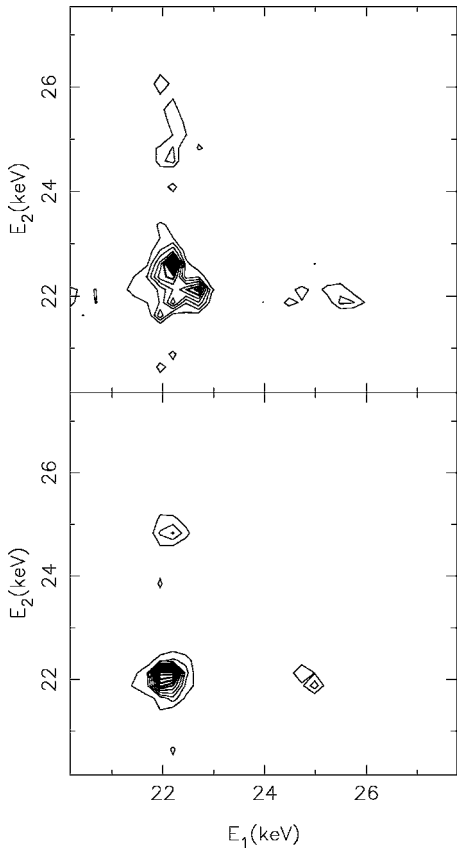

FIG. 6. Prompt (top) and delayed (bottom) coincidence energy spectra in the *K* x-ray region for double *K*-shell photoionization of Ag by 90-keV photons displayed as contour plots of the energy in one detector (E_1) versus that measured in the other (E_2).

x-ray diagram line and the Compton scattered photon. Because of the broad Compton profile of the Ag *K* electrons, this results in a smooth continuous background extending from a relatively high energy (the incident photon energy less the 25.5 keV *K* binding energy) down to zero [44]. This background can be seen in Fig. 4 as the long horizontal and vertical stripes spanning the spectrum in coincidence with the fluorescence and escape lines. In the region of interest (~20–30 keV), this forms a relatively flat background which must be subtracted in the analysis.

It should be noted that all of these coincidence backgrounds contribute to the diagram line intensities in the coincidence spectra and *not* the hypersatellites. Analysis therefore must separate the hypersatellite intensity from the residual *K* diagram lines (and linear Compton background) appearing in the *K*-*K* coincident spectra.

IV. ANALYSIS AND RESULTS

A typical example of the raw data is shown in Fig. 6 for the case of 90-keV incident photon energy. Plotted are the energy spectra in each of the two detectors in the region of the *K* x rays for both prompt and delayed coincidences. In the lower panel, the delayed coincidences represent the accidental coincidence resulting from fluorescent decay of the

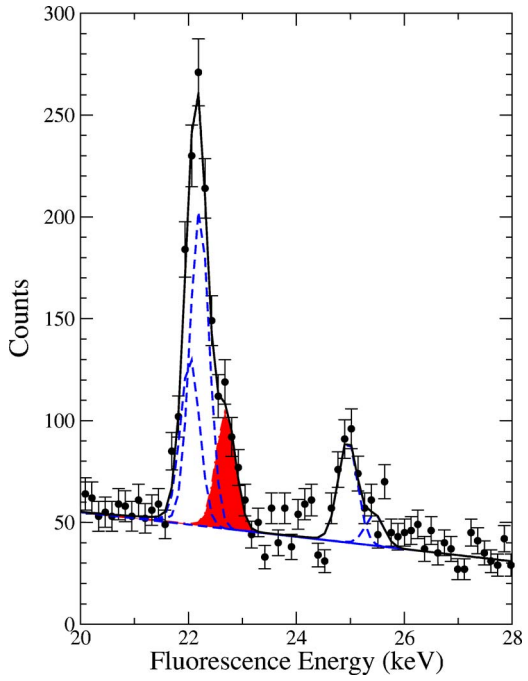

FIG. 7. (Color online) Prompt spectrum measured in Det. 2 in coincidence with *K* x rays in Det. 1 for the case of ionization by 90-keV photons. The solid line is the fit to the data obtained by summing the various components shown as dashed lines for the diagram lines and a shaded peak for the $K^h\alpha$ contribution.

predominant single *K* vacancy states yielding $K\alpha$-$K\alpha$ and $K\alpha$-$K\beta$ diagram lines ($K\beta$-$K\beta$ are also present but too weak to observe on this scale). At this photon energy, which is near the expected peak of the double *K*- shell ionization cross section, the shifted hypersatellite lines are quite apparent in the prompt (upper) spectrum and obviously absent in the lower (delayed) spectrum.

For comparison, in Fig. 7, we show a projection of the prompt coincidence data (upper panel of Fig. 6) onto the E_2 axis. The solid line is a fit to the data. The dashed lines are fits to the background and diagram lines, and the shaded area is a fit to the $K^h\alpha$ contribution.

In Ag, the hypersatellite shifts from the corresponding diagram lines are predicted to be ~535 eV and ~682 eV for the $K^h\alpha$ and $K^h\beta$ groups, respectively [38]. Those shifts are readily apparent in comparing the upper and lower panels of Fig. 6. The separation between $K^h\alpha_1$ and $K^h\alpha_2$ is 174 eV which is only 0.7 eV greater than the separation between $K\alpha_1$ and $K\alpha_2$. It should be noted that the natural linewidth (~10 eV) is a small fraction of the detector resolution (~350 eV) and is therefore neglected in the analysis.

The 90-keV data shown in Figs. 6 and 7 correspond to the highest yield of double *K* vacancies we measured. But even there, the effects of Compton scattering from the *K* shell is apparent in the flat background seen under the peaks in Fig. 7. The Compton backgrounds were problematic particularly near (and below) threshold and simply subtracting the prompt and delayed spectra was not sufficient for cleanly isolating the hypersatellite-satellite coincidences. This is illustrated in Fig. 8 which are data recorded in detector (Det.) 1 at an x ray energy of 61.5 keV. The three panels show a

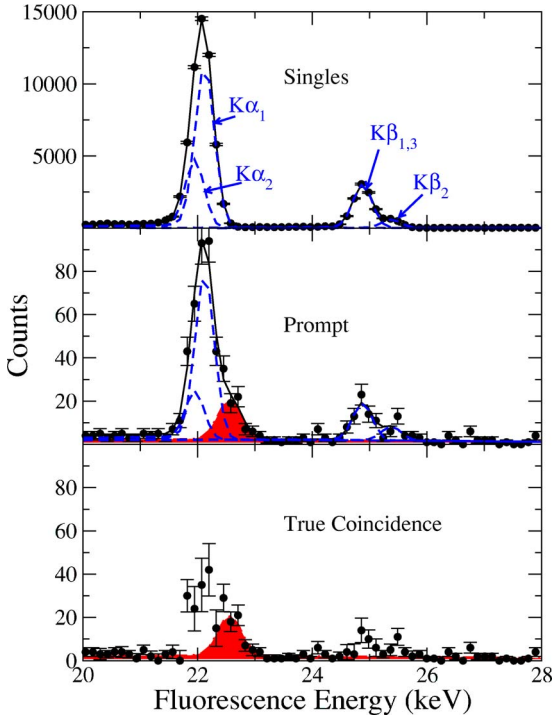

FIG. 8. (Color online) The fluorescence energy spectra detected in one of the detectors for the case of ionization by 61.5-keV photons. Top panel is for "singles" events, middle for prompt coincidences, and bottom are true coincidences obtained by subtracting the delayed coincidence spectrum from the corresponding prompt spectrum. The two lower spectra are obtained for coincidences with K x rays in the other detector. The solid lines are the fits to the data obtained by summing the various components shown as dashed lines for the diagram lines and a shaded peak for the $K^h\alpha$ contribution.

"singles" spectrum, a spectrum in Det. 1 for events in prompt coincidence with a K x ray in Det. 2, and the true coindcidences. The latter are obtained by subtracting the spectrum of delayed events ("randoms") from the prompt coincidences (middle panel). The problem is that the true coincidence spectrum (lower panel) shows residual counts near the position of the diagram lines $K\alpha_1$ and $K\alpha_2$. These counts are true coincidences between the continuum in the other detector (Det. 2) due to Compton scattering (off the K shell) and the associated diagram line in Det. 1 from the filling of the resulting K hole. To overcome this problem we do not use the true coincidence spectrum to determine the hypersatellite intensities but rather adopt the following proceedure which uses the top two spectra in Fig. 8:

(i) First, the diagram lines were fitted in the "singles" spectra constructed for each detector from those events in which only a single photon was detected. The line shapes were optimized using the GELIFIT program incorporating characteristic low-energy tails to account for incomplete charge collection [45]. Included diagram lines were $K\alpha_1$, $K\alpha_2$, $K\beta_{1,3}$, and $K\beta_2$.

(ii) Then, those fits were combined with an additional broader line (though all other line shape parameters were fixed) at the expected mean energy of the $K^h\alpha_{1,2}$. The width of this peak corresponds to a blending of the $K^h\alpha_1$ and $K^h\alpha_2$ hypersatellite lines which are separated by 174 eV. The relative ratios of the hypersatellite and diagram lines were then varied to best-fit the prompt coincidence spectrum. Because of the ~350-eV resolution of the detectors, any satellite intensity is included in the diagram lines.

This procedure circumvents the problem of the Compton background and has the advantage that the errors are determined by the fitting procedure.

Summing those yields for each detector produces the quantity $I_{2K}(\alpha)$. Similarly sums were carried out on the singles spectra for the normal Kα diagram lines to yield the integrated intensity $I_{1K}(\alpha)$ for the predominant single vacancy transitions. These intensities can be related to the corresponding vacancy probabilities through

$$I_{2K}(\alpha) = fN_{2K}\omega_{2K}\omega_{1K}\epsilon_1\epsilon_2\frac{\Omega_1\Omega_2}{16\pi^2} \tag{2}$$

and

$$I_{1K}(\alpha) = fN_{1K}\omega_{1K}\frac{\epsilon_1\Omega_1 + \epsilon_2\Omega_2}{4\pi}, \tag{3}$$

where N_{nK} is the total number of atoms produced with n K vacancies and ω_{nK} is the corresponding fluorescence yield. The fractionation factor f represents the fraction of all K x rays in the Kα group. The absolute photopeak detector efficiencies are given by ϵ_i and solid angles by Ω_i. In deriving Eqs. (2) and (3) we have assumed that the $K\beta$:$K\alpha$ ratios are the same for the diagram and hypersatellite lines. The similarity of these ratios has been suggested by Briand *et al.* [46] and is consistent with the Fe data of Diamant *et al.* [24] who measureed a $K^h\beta/K^h\alpha$ ratio of about 0.1 in agreement with the ratio (0.12) expected for the diagram lines [47]. We assign an uncertainty of 2% to our final result to account for the uncertainty in $K^h\beta/K^h\alpha$.

From Eqs. (2) and (3), the ratio of double to single ionization of the K shell can be expressed as

$$R = \frac{N_{2K}}{N_{1K}} = \frac{4\pi}{\omega_{2K}}\frac{I_{2K}}{I_{1K}}\left(\frac{1}{\epsilon_1\Omega_1} + \frac{1}{\epsilon_2\Omega_2}\right). \tag{4}$$

The cross section for double K-shell photoionization (σ_{KK}) can be expressed in terms of the total ionization cross section for the K shell as

$$\sigma_{KK} = P_{KK}(\sigma_K + \sigma_{KK}) \tag{5a}$$

$$\simeq P_{KK}\sigma_K, \tag{5b}$$

where P_{KK} is the Bayesian conditional probability that a double K vacancy is created given that the K shell is ionized [48] and σ_K the cross section for single K ionization. This, of course, presumes that $\sigma_{KK} \ll \sigma_K$ in which case

$$P_{KK} = \frac{\sigma_{KK}}{\sigma_K} = R. \tag{6}$$

Although the fluorescence yields for double-K-hole states in light atoms can be substantially higher than those of single vacancy states, Chen has calculated [49] that for $Z > 25$ they are identical to a good approximation ($<1\%$ difference for

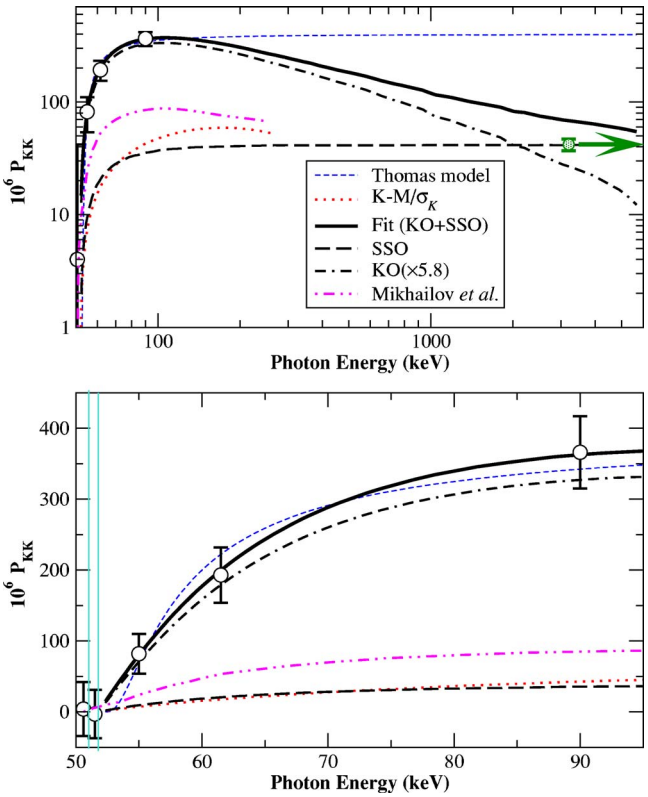

FIG. 9. (Color online) The ratio of double to single *K*-shell ionization of silver as a function of incident photon energy. The upper panel shows the data on a log-log plot while the lower panel shows the same data with linear scales, for the lower-energy region covered by this experiment. The open circles are the present results while the shaded circle shows the EC result of Ko *et al.* [27] which represents the asymptotic limit as is indicated by the arrow in the upper panel. The various model calculations are indicated in the legend. The "Fit", "SSO", and "KO" curves are based on the Rost model (see text). In the lower panel, the two vertical lines indicate the thresholds $2E_{1K}$ and E_{2K} described in the text. See text for explanations of the other curves.

Z=47). Thus, we assume $\omega_{2K}=\omega_{1K}=0.830(25)$ in silver [40]. As described above, the products of the solid angles and absolute efficiencies of each Ge detector ($\epsilon_n\Omega_n$), including transmission through the Kapton filters (0.9939), were determined in independent source measurements. Self-absorption in the Ag target was several orders of magnitude smaller and was neglected. Including these numbers in Eq. (4) with the measured yields, we determined the probability P_{KK} at each incident photon energy and those results are shown in Fig. 9 and Table I. The estimated 1σ errors include the propagation of contributions from counting statistics, background subtraction, fitting errors, efficiency measurements, and uncertainty in the fluorescence yield. We also considered the possibility of an angular correlation between the two photons but this leads to a negligible correction to our results [50].

V. DISCUSSION

The results shown in Fig. 9, in addition to our photoionization data (open circles), include the EC data of [27] for the asymptotic limit. The thin-dashed curve shows a best fit to our data using the Thomas model [51]. This model, which has been used in the past to describe shake processes near threshold [23], uses time-dependent perturbation theory and produces a simple expression for the energy dependence which depends only on the radius and binding energy of the shaken electron. In this model, the probability P_{KK} is expressed as

$$P_{KK}(\varepsilon) = P_{KK}(\infty)\exp\left(-\frac{m_e r^2\Lambda^2}{2\hbar^2\varepsilon}\right), \tag{7}$$

where r is the radius of the K shell, Λ is the binding energy of the shaken electron (26.268 keV), m_e the electron mass, and $\varepsilon=E_\gamma-E_{2K}$ is the excess excitation energy carried by the two photoelectrons for photon energy E_γ. The best fit of this expression to our data gives r=0.0112 Å and $P_{KK}(\infty)=3.97\times10^{-4}$ with fitting errors of about 10%. The K shell radius is consistent with the hydrogenic value of 0.0113 Å. Because it completely neglects the strong energy dependence of the KO contribution near threshold, the model predicts a rise to an asymptotic limit an order of magnitude higher than the EC result of $4.2(5)\times10^{-5}$ [27].

TABLE I. Measured values of P_{KK} in silver and incident photon energies (E_γ) above the single (E_{1K}) and double K (E_{2K}) K-shell ionization thresholds. All energies are in keV. $P_{KK}(\infty)$ is obtained from the EC results [27].

E_γ	E_γ-E_{1K}	E_γ-E_{2K}	10^6P_{KK}
50.6	25.1	−1.2	4(38)
51.5	26.0	−.3	−3(34)
55.0	29.5	3.2	82(28)
61.5	36.0	9.7	193(39)
90.0	64.5	38.2	366(51)
∞	∞	∞	42(5)

A more physical view of the results can be obtained by using the σ_{KK} scaling law given by Kornberg and Miraglia (KM) [53] for double ionization of He-like ions and dividing that cross section by the single K-shell ionization cross section [54]. KM used both correlated (C3) and uncorrelated (C2) two-electron continuum wave functions to calculate the energy and Z dependence of the double photoionization cross section for heliumlike ions. Their calculations with the correlated C3 wave functions underestimate the He data by orders of magnitude [55] but are valid at asymptotically high energies where they agree quite well with the result using the independent-electron approximation of the uncorrelated C2 model. Using their velocity gauge C2 result, we obtain the dotted line in Fig. 9 labeled "KM/σ_K." This result neglects final-state e-e interactions, so it fails to account for the dynamical contribution that is important at low energies. It merely represents the shake-off contribution and lies much lower than the observations.

It should be noted that the asymptotic limit indicated in Figs. 9 (and Fig. 10) refers only to the photoelectric effect. Compton scattering from the K shell can also produce double

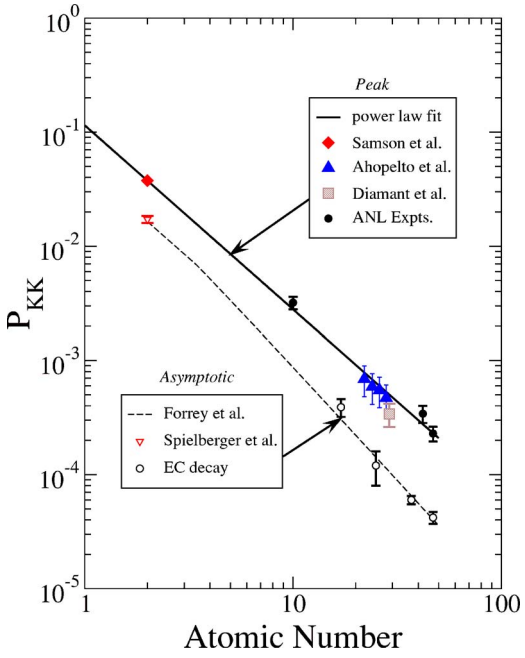

FIG. 10. (Color online) The ratio of double to single *K*-shell photoionization as a function of atomic number. The solid symbols are used for experiments carried out in the region of the predicted peak in the double photoionization cross section. The open symbols are used for measurements of the ratio in the asymptotic limit, and the corresponding theoretical prediction for the asymptote [52] is shown as a dashed curve. The ANL experiments include an interpolation of the present $Z=47$ Ag results as described in the text as well as our $Z=10$ Ne [26] and $Z=42$ Mo [22] results. Also shown (solid line) is our previous $1/Z^{1.61}$ power-law fit.

K vacancies but this process is distinguishable by its different final state. Although we do not distinguish between the two processes in our experiment, the contribution from Compton scattering is negligible because the cross section for Compton scattering from the *K* shell is more than two orders of magnitude smaller than photoionization at our highest energy of 90 keV [56].

The *ab initio* calculation which comes closest to the data is the recent result of Mikhailov *et al.* [57,58] shown by the double-dotted chained curve in Fig. 9. They use QED perturbation theory through leading orders of $1/Z$ and αZ expansions to calculate the energy dependence of double ionization of heliumlike ions. That result is intermediate between the KM curve and our data, but shows a peak ~100 keV with a gentle falloff towards the asymptote, qualitatively consistent with the data but requiring scaling by a factor of 4 to come into agreement with it. Mikhailov *et al.* [58] suggest that the discrepancies with experiment may be due to relativistic effects such as spin-orbit coupling, which are not included in their calculation.

Recently, Rost and his collaborators have suggested an alternative way to treat this problem [33,35]. They treat shake-off (SSO) as the purely quantum-mechanical process that it represents. The dynamical KO is treated quasiclassically and then added *incoherently* to the SSO result. The justification for this is that interferences play a minor role because SO and KO are almost orthogonal with respect to their angular characteristics [35]. Taking their result and independently scaling their SSO and KO results before adding them together, we obtain the solid curve in Fig. 9. For the energy axis, we have scaled the excess excitation energy by Z^2 [53]. Scaling of P_{KK} was treated differently. Scaling the SSO and KO contributions by $1/Z^2$ produces an asymptotic value of 2.98×10^{-5} which is somewhat smaller than the experimental EC value of $4.2(5)\times10^{-5}$ described earlier. We therefore rescaled both SSO and KO by a factor of 1.41 to exactly match the asymptote. This rescaled SSO (long dashed line in Fig. 9) is seen to be in excellent agreement with the KM result (dotted line). Finally, an additional arbitrary rescaling factor for the KO term was then applied to best fit our data (solid line). This factor was found to be 5.8(7) with a normalized $\chi^2=1.2$.

Because of the dominance of the KO term in the region of the broad maximum, it is instructive to plot the trend of P_{KK} in the peak region with Z as we suggested a few years ago [22]. It should be noted that because the asymptotic region is at so high an energy in all but the lightest atoms and the yield is so low near threshold, most previous measurements have tended to be carried out in the region of the broad maximum in the double *K*-shell ionization cross section. Combining all of the available data, including our previous measurements on Ne [26], Mo [22], and the present Ag result, we show that trend in Fig. 10. We also show in Fig. 10 the earlier photoionization results [21] in lighter atoms ($22\leqslant Z\leqslant 28$) as well as the He result of Samson *et al.* [5]. Those measurements were also carried out somewhat above threshold but well below the asymptotic regime and roughly in the region of the broad maximum of the double ionization cross section at an excess energy above threshold of $\sim 0.01\times Z^2$ keV as predicted by the KM scaling laws [53]. For silver, that corresponds to a photon energy of 73.1 keV, so for the $Z=47$ experimental result in Fig. 10 we have plotted the interpolation of our data to that energy which gives $P_{KK}^{\mathrm{peak}}=2.29(34)\times10^{-4}$.

Shake processes lead to a $1/Z^2$ falloff in the double *K*-shell ionization probability [59] and that is a predominant characteristic of all of the *Z*-scaling laws suggested for He-like ions. For comparison, we show in Fig. 10 one of those scaling laws by Forrey *et al.* [52]. It shows excellent agreement with the asymptotic ratios measured in He by [60] and by the EC measurements in Ag [27], Cl ($Z=17$) [61], Mn ($Z=25$) [62], and Rb ($Z=37$) [63]. In contrast, those measurements in the peak region, besides being obviously systematically higher, also fall off significantly slower than the $1/Z^2$ dependence of shake-off. Surprisingly, all of the newer data show good agreement with the somewhat weaker $1/Z^{1.61}$ dependence which we reported earlier [22]. This result and the above findings requiring rescaling of the Rost group's KO contribution suggest that KO may in fact become *more* important with increasing *Z*.

This finding is shown schematically in Fig. 11. We define the power-law fit to the peak regions to be a function $Y_p(Z)$ and the asymptotic dependence of Forrey *et al.* [52] is similarly represented by $Y_a(Z)$. Since the former includes both KO and SSO contributions while the latter is only SSO, then the ratio $[Y_p(Z)-Y_a(Z)]/Y_a(Z)$ is a measure of the KO and

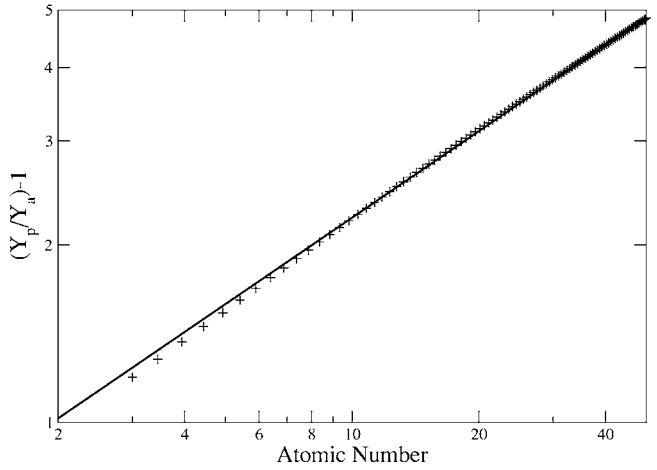

FIG. 11. The dimensionless ratio of $(Y_p - Y_a)/Y_a$ as described in text. The + symbols show that ratio computed using the power law fit for Y_p and the asymptotic expression of [52] for Y_a. The solid line is a best fit to those points.

SSO relative contributions. That ratio is plotted in Fig. 11. We have best-fitted that ratio to a power law of the form $a_0 Z^p$ (solid line in the figure) and found $p=0.49$, very close to the $\sqrt{Z}$ dependence.

What is the origin of this Z dependence? As was first pointed out by Samson in his investigation of double ionization of atoms [64], the knockout contribution is proportional to the electron-impact ionization cross section (σ_{ee}) and the electron density sampled by the photoionized electron. For our case of double K-shell ionization, the peak value of σ_{ee} can be estimated from the phenomenological Lotz formula [65] to vary with Z^{-4}. More recently, Santos *et al.* reported the results of calculations of σ_{ee} with the relativistic binary-encounter Bethe (BEB) model [66]. Fitting the peak values they report, we find a somewhat steeper $Z^{-4.3}$ dependence. To correct for the fact that σ_{ee} represents a full reaction cross section while in double ionization the impacting electron is already inside the atom, we follow the prescription of Samson [64] and scale that cross section by the electron density sampled by the photoionized electron and by the ratio of path lengths of the impacting electrons for both photoionization and electron impact ionization. If we define the latter as ℓ_e, then the KO contribution to P_{KK} should be proportional to

$$P_{KK}(\mathrm{KO}) \propto \frac{\sigma_{ee}}{\ell_e} \int_0^\infty |\psi_{1s}(r)|^2 dr, \tag{8}$$

where ψ_{1s} is the wave function for the residual K-shell electron. The integral represents the K-shell electron density integrated over the path length of the exiting electron trajectory and, assuming a hydrogenic wave function, is proportional to Z^2. Assuming the BEB result for σ_{ee}, a hydrogenic $1/Z$ dependence for ℓ_e, and the $1/Z^2$ behavior for shake-off, the net result is

$$\frac{P_{KK}(\mathrm{KO})}{P_{KK}(\mathrm{SSO})} \propto Z^{0.7}, \tag{9}$$

suggesting a slow growth with Z, similar to the $\sqrt{Z}$ dependence of that ratio in Fig. 11.

The energy dependence of P_{KK} in this model is also illuminating. The energy dependence of P_{KK} originates entirely from σ_{ee}. Using the Lotz formula, we expect the peak of σ_{ee} at an electron energy E_e such that $E_e/I=e$ where I is the binding of the residual K electron and e is the natural logarithm base. Assuming the binding energies of the two K electrons are the same, then the corresponding peak in photon energy E_γ would occur at

$$E_\gamma = E_e + I \tag{10a}$$

$$= I(1+e) \tag{10b}$$

$$\simeq 50.6 Z^2 \text{ eV}, \tag{10c}$$

which for Ag corresponds to 112 keV, in good agreement with the trend of the data suggested by Fig. 9. Because the single ionization cross section asymptotically falls as $E_e^{-7/2}$, the peak of P_{KK} should be shifted to higher energy than the predicted peak of σ_{KK} [53] and that is indeed what we find.

VI. SUMMARY

This work has demonstrated that it is now possible, with modern third-generation synchrotron sources, to explore the energy dependence of double K-shell ionization in heavy atoms. We have measured the ratio of double to single photoionization of the K shell for neutral Ag atoms from threshold to near the expected peak as a function of x-ray energy. There is a need for theoretical calculations for this process in heavy atoms. Such calculations would explore the interesting but challenging regime where both electron-electron interactions and relativity are simultaneously important. For lack of such theoretical results we have compared our data with scaling results calculated for He. We find it is necessary to include the contribution from dynamical electron-electron scattering, or knockout, in the near-threshold region. In future work it would be desireable to extend these measurements to the higher-energy regime to characterize the peak in the ratio given in Fig. 9. We also analyzed the Z dependences of the existing data on double K-shell photoionization. This analysis suggests that the KO contribution is more important at higher Z than was expected based on extrapolating theoretical results from lower Z. This points to the desirability of experiments and theoretical work at high Z.

ACKNOWLEDGMENTS

We thank J. Greene for preparation of the various target samples and the BESSRC staff (M. Beno, M. Engbretson, G. Jennings, C.A. Kurtz, and J. Linton) for assistance with the beamlines. This work was supported by the Chemical Sciences, Geosciences, and Biosciences Division, the Division of Nuclear Physics, and (in the case of the Advanced Photon Source) the Office of Basic Energy Sciences, Office of Science, U.S. Department of Energy, under Contract No. W-31-109-Eng-38.

[1] T. A. Carlson, Phys. Rev. **156**, 142 (1967).

[2] E. U. Condon and G. H. Shortley, *The Theory of Atomic Spectra* (Cambridge University Press, London, 1970).

[3] *Atomic Inner-Shell Physics*, edited by B. Crasemann, (Plenum, New York, 1985), Chap. 7.

[4] J. H. McGuire, N. Berrah, R. J. Bartlett, J. A. R. Samson, J. A. Tanis, C. L. Cocke, and A. S. Schlachter, J. Phys. B **28**, 913 (1995).

[5] J. A. R. Samson, W. C. Stolte, Z. -X. He, J. N. Cutler, Y. Lu, and R. J. Bartlett, Phys. Rev. A **57**, 1906 (1998).

[6] M. S. Lubell, Nucl. Instrum. Methods Phys. Res. B **99**, 177 (1995).

[7] J. P. Briand, P. Chevallier, A. Chetioui, J. P. Rozet, M. Tavernier, and A. Touati, Phys. Rev. A **23**, 39 (1981).

[8] H. G. Berry, R. W. Dunford, and A. E. Livingston, Phys. Rev. A **47**, 698 (1993).

[9] W. Heisenberg, Z. Phys. **32**, 841 (1925).

[10] A. Migdal, J. Phys. (Moscow) **4**, 449 (1941).

[11] E. L. Feinberg, J. Phys. (Moscow) **4**, 423 (1941).

[12] G. Charpak, Compt. Rend. **237**, 243 (1953).

[13] M. S. Freedman, Annu. Rev. Nucl. Sci. **24**, 209 (1974).

[14] J. P. Briand, P. Chevallier, M. Tavernier, and J. P. Rozet, Phys. Rev. Lett. **27**, 777 (1971).

[15] J. P. Briand, A. Touati, M. Frilley, P. J. Chevallier, A. Johnson, J. P. Rozet, M. Tavernier, S. Shafroth, and M. O. Krause, J. Phys. B **9**, 1055 (1976).

[16] T. Mukoyama and S. Shimizu, Phys. Rev. C **11**, 1353 (1975).

[17] J. Rangama, D. Hennecart, N. Stolterfoht, J. A. Tanis, B. Sulik, F. Fremont, X. Husson, and J. -Y. Chesnel, Phys. Rev. A **68**, 040701(R) (2003).

[18] P. Richard, W. Hodge, and C. F. Moore, Phys. Rev. Lett. **29**, 393 (1972).

[19] O. Benka, R. L. Watson, and B. Bandong, Phys. Rev. A **28**, 3334 (1983).

[20] O. Keski-Rahkonen, J. Saijonmaa, M. Suvanen, and A. Servomaa, Phys. Scr. **16**, 105 (1977).

[21] J. Ahopelto, E. Rantavuori, and O. Keski-Rahkonen, Phys. Scr. **20**, 71 (1979).

[22] E. P. Kanter, R. W. Dunford, B. Krässig, and S. H. Southworth, Phys. Rev. Lett. **83**, 508 (1999).

[23] R. Diamant, S. Huotari, K. Hämäläinen, C. C. Kao, and M. Deutsch, Phys. Rev. Lett. **84**, 3278 (2000).

[24] R. Diamant, S. Huotari, K. Hämäläinen, C. C. Kao, and M. Deutsch, Phys. Rev. A **62**, 052519 (2000).

[25] M. Oura *et al.* J. Phys. B **35**, 3847 (2002).

[26] S. H. Southworth, E. P. Kanter, B. Krässig, L. Young, G. B. Armen, J. C. Levin, D. L. Ederer, and M. H. Chen, Phys. Rev. A **67**, 062712 (2003).

[27] S. K. Ko, H. J. Cho, and S. K. Nha, Nucl. Phys. A **641**, 49 (1998).

[28] S. L. Carter and H. P. Kelly, Phys. Rev. A **24**, 170 (1981).

[29] H. P. Kelly, in *Atomic Inner-Shell Processes*, edited by B. Crasemann (Academic Press, New York, 1975), Chap. 8, pp. 331–352.

[30] T. N. Chang and R. T. Poe, Phys. Rev. A **11**, 191 (1975).

[31] K. I. Hino, T. Ishihara, F. Shimizu, N. Toshima, and J. H. McGuire, Phys. Rev. A **48**, 1271 (1993).

[32] A. S. Kheifets and I. Bray, Phys. Rev. A **57**, 2590 (1998), and references therein.

[33] T. Schneider, P. L. Chocian, and J. -M. Rost, Phys. Rev. Lett. **89**, 073002 (2002).

[34] L. I. Schiff, *Quantum Mechanics* (McGraw-Hill, New York, 1968).

[35] T. Schneider and J. -M. Rost, Phys. Rev. A **67**, 062704 (2003).

[36] T. Åberg, Phys. Rev. A **2**, 1726 (1970).

[37] R. Krivec, M. Y. Amusia, and V. B. Mandelzweig, Phys. Rev. A **62**, 064701 (2000).

[38] M. H. Chen, B. Crasemann, and H. Mark, Phys. Rev. A **25**, 391 (1982).

[39] O. Keski-Rahkonen and M. O. Krause, At. Data Nucl. Data Tables **14**, 139 (1974).

[40] W. Bambynek, B. Crasemann, R. W. Fink, H. -U. Freund, H. Mark, C. D. Swift, R. E. Price, and P. V. Rao, Rev. Mod. Phys. **44**, 716 (1972).

[41] M. A. Beno, M. Engbretson, G. Jennings, G. S. Knapp, J. Linton, C. Kurtz, U. Rütt, and P. A. Montano, Nucl. Instrum. Methods Phys. Res. A **467-468**, 699 (2001).

[42] K. Ilakovac, J. Tudorić-Ghemo, and S. Kaučić, Phys. Rev. A **44**, 7392 (1991).

[43] X. Long, M. Liu, F. Ho, and X. Peng, At. Data Nucl. Data Tables **45**, 353 (1990).

[44] V. Marchetti and C. Franck, Phys. Rev. Lett. **59**, 1557 (1987).

[45] D. C. Radford, URL http://radware.phy.ornl.gov/gf3/gf3.html

[46] J. P. Briand, P. J. Chevallier, A. Johnson, J. P. Rozet, M. Tavernier, and A. Touati, Phys. Fenn. **9**(S1), 409 (1974).

[47] J. H. Scofield, At. Data Nucl. Data Tables **14**, 121 (1974).

[48] D. S. Sivia, *Data Analysis* (Clarendon Press, Oxford, 1996).

[49] M. H. Chen, Phys. Rev. A **44**, 239 (1991).

[50] We estimated the angular correlation between the two coincident photons using formulas in Balashov *et al.*, *Polarization and Correlation Phenomena in Atomic Collisions* (Kluwer Academic, New York, 2000), assuming that the 5*s* valence electron plays no role. Although the $J=1$ intermediate states have an alignment of $1/\sqrt{2}$, the opening angle correlations almost cancel in the sum over final $J=0,1$, and 2 states and the net effect is negligible at our level of accuracy.

[51] T. D. Thomas, Phys. Rev. Lett. **52**, 417 (1984).

[52] R. C. Forrey, H. R. Sadeghpour, J. D. Baker, J. D. MorganIII, and A. Dalgarno, Phys. Rev. A **51**, 2112 (1995).

[53] M. A. Kornberg and J. E. Miraglia, Phys. Rev. A **49**, 5120 (1994).

[54] S. Puri, B. Chand, D. Mehta, M. L. Garg, N. Singh, and P. N. Trehan, At. Data Nucl. Data Tables **61**, 289 (1995).

[55] M. A. Kornberg and J. E. Miraglia, Phys. Rev. A **48**, 3714 (1993).

[56] E. Storm and H. Israel, Nucl. Data, Sect. A **A7**, 566 (1970).

[57] A. I. Mikhailov, I. A. Mikhailov, A. V. Nefiodov, G. Plunien, and G. Soff, Pis'ma Zh. Eksp. Teor. Fiz. **78**, 141 (2003), [JETP Lett. **78**, 110 (2003)]

[58] A. I. -Mikhailov, I. A. Mikhailov, A. N. Moskalev, A. V. Nefiodov, G. Plunien, and G. Soff, Phys. Rev. A **69**, 032703 (2004).

[59] J. S. Levinger, Phys. Rev. **90**, 11 (1953).

[60] L. Spielberger *et al.*, Phys. Rev. Lett. **74**, 4615 (1995).
[61] J. A. Miskel and M. L. Perlman, Phys. Rev. **94**, 1683 (1954).
[62] J. P. Briand, P. J. Chevallier, A. Johnson, J. P. Rozet, M. Tavernier, and A. Touati, Phys. Lett. **49A**, 51 (1974).
[63] G. Schupp and H. J. Nagy, Phys. Rev. C **29**, 1414 (1984).
[64] J. A. R. Samson, Phys. Rev. Lett. **65**, 2861 (1990).
[65] W. Lotz, Z. Phys. **232**, 101 (1970).
[66] J. P. Santos, F. Parente, and Y. -K. Kim, J. Phys. B **36**, 4211 (2003).